nature climate change

ARTICLES

https://doi.org/10.1038/s41558-020-00957-9

Nature Climate Change, 2020

Check for updates

Stringent mitigation substantially reduces risk of unprecedented near-term warming rates

Christine M. McKenna[1]✉, Amanda C. Maycock[1], Piers M. Forster[1], Christopher J. Smith[1,2] and Katarzyna B. Tokarska[3]

Following the Paris Agreement, many countries are enacting targets to achieve net-zero GHG emissions. Stringent mitigation will have clear societal benefits in the second half of this century by limiting peak warming and stabilizing climate. However, the near-term benefits of mitigation are generally thought to be less clear because forced surface temperature trends can be masked by internal variability. Here we use observationally constrained projections from the latest comprehensive climate models and a simple climate model emulator to show that pursuing stringent mitigation consistent with holding long-term warming below 1.5 °C reduces the risk of unprecedented warming rates in the next 20 years by a factor of 13 compared with a no mitigation scenario, even after accounting for internal variability. Therefore, in addition to long-term benefits, stringent mitigation offers substantial near-term benefits by offering societies and ecosystems a greater chance to adapt to and avoid the worst climate change impacts.

Near-term warming rates affect how rapidly societies and ecosystems must adapt to the worst impacts of climate change. Recent decades have seen high rates of warming in global mean surface air temperature (GSAT); the maximum warming trend for 20-year segments of the observation-based record since pre-industrial times is 0.27 °C per decade, which occurred in the past few decades with the exact timing dependent on the dataset used (Supplementary Fig. 1). It is clear that to stabilize climate in the long term, global net-zero GHG emissions must be achieved[1]; however, it is less clear when the benefits of mitigation applied now will become evident[2–6].

Here, we investigate the effect of different levels of mitigation in future emission scenarios on surface warming rates in the next 20 years (2021–2040), a key period for policymakers at the forefront of climate change adaptation. For example, crop breeding is unlikely to keep pace with climate impacts on agriculture over this period under current rates of warming[7]. The next 20 years is also a typical time horizon for initial planning to operation of large-scale structural responses to support climate change adaptation, such as the design and implementation of flood defences[8].

The consensus is that differences in GSAT between high and low emission pathways emerge only after the 2050s, with changes not being detectable beforehand[2–6]. The long atmospheric lifetime of CO_2 means that substantial emission reductions are needed to alter the upward trend in atmospheric concentration and effective radiative forcing (ERF)[9], making it difficult for society to notice the immediate benefits of mitigation efforts. The Paris Agreement long-term targets are concerned with addressing the anthropogenic warming contribution[10,11], but the temperature changes that society will experience in the near term will come from a combination of a forced response to radiative forcings and internal climate variability[12,13]. On decadal timescales, internal variability can overwhelm the forced climate response, even for spatially averaged quantities such as global temperature[4], having profound implications for the public understanding of climate change. For example, the period of relatively slow surface warming between 1998 and 2012, which was partly associated with internal climate variability[14], was widely misreported, leading to doubt in the public mind about how well anthropogenic climate change is understood[15]. It is therefore important to communicate to what extent strong mitigation efforts will offer benefits in the near term as well as in the long term, and to what extent those benefits may be masked on shorter timescales by internal variability.

Here, we combine two approaches (Methods) to assess whether mitigation has detectable benefits for near-term warming rates. The first approach uses projections from the latest Coupled Model Intercomparison Project Phase 6 (CMIP6) models, driven by Shared Socioeconomic Pathway (SSP[16]) scenarios and constrained according to their representation of recent observed warming rates[17]. The second approach uses a simple climate model emulator (the Finite amplitude Impulse Response (FaIR) model[18]), with added observation-based estimates of internal variability[19], also run under SSP scenarios as well as a scenario consistent with the current and projected pledges as of 2019 in the nationally determined contributions (NDCs) under the Paris Agreement[20–22]. Simple climate models such as FaIR are designed to emulate the behaviour of more complex climate models in a computationally inexpensive way, by using simplified representations of the physical relationships between emissions, atmospheric concentrations of GHGs and other climate forcers, radiative forcing, and temperature change. The combination of these two approaches is advantageous because the CMIP6 models, while comprehensive, do not necessarily accurately represent observed internal variability, and CMIP6 was not designed to fully sample the range of parameter uncertainties that affect temperature projections. Since FaIR is inexpensive to run, it can be used to more broadly sample uncertainty in temperature projections than individual complex climate models (Methods).

We focus on strong mitigation pathways in line with the Paris Agreement 1.5 °C and 2 °C long-term temperature targets (SSP1-1.9 and SSP1-2.6, respectively) and include the NDC-like scenario to consider a less ambitious and more plausible mitigation pathway[23]. These are compared with baseline no mitigation pathways

[1]School of Earth and Environment, University of Leeds, Leeds, UK. [2]International Institute for Applied Systems Analysis (IIASA), Laxenburg, Austria. [3]Institute for Atmospheric and Climate Science, ETH Zurich, Zurich, Switzerland. ✉e-mail: C.McKenna1@leeds.ac.uk

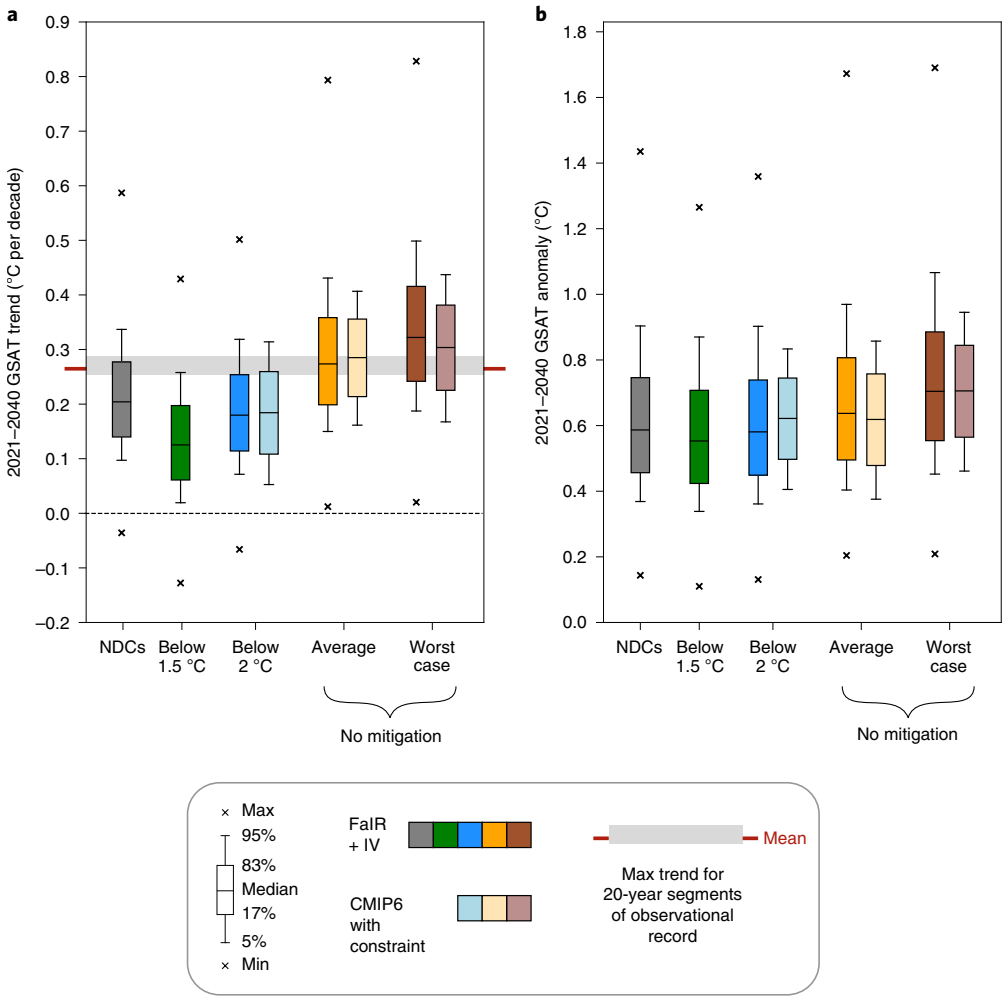

Fig. 1 | Near-term (2021–2040) GSAT trends and anomalies relative to the near-present-day (1995–2014) baseline. a, Trends in °C per decade. **b**, Anomalies in °C. The data are shown for pathways consistent with current and projected NDCs (grey box); highest-ambition mitigation in line with the Paris Agreement target to pursue efforts to keep warming to below 1.5 °C (SSP1-1.9, green box); strong mitigation in line with the Paris Agreement target to keep warming below 2 °C (SSP1-2.6, blue boxes); average no mitigation baseline scenario (SSP3-7.0, orange boxes); and unlikely worst-case no mitigation scenario (SSP5-8.5, brown boxes). The lighter shading shows the CMIP6 projections with a historical constraint applied, and the darker shading shows the FaIR projections plus an observation-based estimate of internal variability (IV) (Methods). The boxes denote the 17–83% range (66% probability), and the whiskers denote the 5–95% range (90% probability) of the projections. The maximum and minimum values are shown as crosses. The maximum trend for 20-year segments of the observation-based record is 0.27 °C per decade (the red ticks on the *y* axes) on the basis of the mean of four datasets, with a range across datasets of 0.25–0.29 °C per decade (grey horizontal bar; 0.25 °C per decade for 2000–2019 in GISTEMPv4, 0.26 °C per decade for 1984–2003 in CWv2 and BE, and 0.29 °C per decade for 1984–2003 in HadCRUT4.6; Supplementary Fig. 1). To compare with the model-simulated GSAT projections, the observation data have been converted from global blended surface temperature (GBST) to GSAT using a scaling factor of 1.087 for BE, CWv2 and GISTEMPv4, and 1.19 for HadCRUT4.6 (Methods).

(SSP3-7.0 and SSP5-8.5). SSP5-8.5 is a highly unlikely worst-case no mitigation pathway since, for example, it assumes a fivefold increase in coal use by the late twenty-first century[23]. SSP3-7.0 represents an average no mitigation pathway[23]; as such, we focus on this pathway as a baseline.

We first ask whether over the next 20 years, mitigation (relative to a baseline of no mitigation) will reduce (1) the risk of experiencing unprecedented warming rates (exceeding the highest warming rate observed to date) and (2) the potential magnitude of extreme warming rates (that is, low-probability 20-year trends in the upper fifth percentile), which could lead to the failure of adaptation plans.

Both the CMIP6 and FaIR simulations show a clear benefit of strong mitigation in terms of decreasing near-term warming rates (Fig. 1a). The following results are quoted from the FaIR projections accounting for internal variability, but note that the distributions of trends for the constrained CMIP6 models are in good agreement with FaIR (Fig. 1a). In the strong mitigation scenario consistent with warming of below 2.0 °C by 2100 (SSP1-2.6; blue boxes), the median warming rate is almost half that in the worst-case no mitigation scenario (SSP5-8.5; brown boxes) and two-thirds that in the average no mitigation scenario (SSP3-7.0; orange boxes). Under the even stronger mitigation scenario consistent with keeping long-term warming below 1.5 °C (SSP1-1.9; green box), the median warming rate is almost one-third of that in the worst-case no mitigation scenario and just over half that in the average no mitigation scenario. Even under less ambitious mitigation consistent with the current and projected NDCs (grey box), there is still a reduction in the median warming rate by around one-third compared with SSP5-8.5 and one-quarter

compared with SSP3-7.0. The median ERF trend in FaIR over this period differs by 0.63 W m^{-2} per decade between SSP1-1.9 and SSP5-8.5 (Supplementary Table 1), which comes mainly from carbon dioxide (0.42 W m^{-2} per decade), methane (0.15 W m^{-2} per decade), tropospheric ozone (0.13 W m^{-2} per decade) and other well-mixed GHGs (0.05 W m^{-2} per decade), with a slight offset from anthropogenic aerosols (−0.16 W m^{-2} per decade). The difference in the near-term total ERF trend is 0.29 W m^{-2} per decade between SSP1-2.6 and SSP3-7.0 (Supplementary Table 1). Over the next 20 years, the difference in median ERF trends between the strong mitigation and no mitigation SSP scenarios are therefore comparable to, or larger than, the total ERF trend over the recent past (1995–2014; 0.40 W m^{-2} per decade; Supplementary Table 1).

Comparing the distributions of projected warming rates with the maximum trend for 20-year segments of the observation-based record since the pre-industrial era (the red ticks on the *y* axes, Fig. 1a), we find that strong mitigation has a discernible effect on the risk of experiencing stronger warming than observed in the past, even after accounting for internal variability. Under SSP1-1.9 (SSP1-2.6), there is only a 4% (14%) probability of the warming rate in the next 20 years exceeding the maximum observed trend, while for SSP3-7.0 (SSP5-8.5), this increases considerably to a 54% (75%) probability. Less ambitious mitigation, in line with the current and projected NDCs, results in a higher probability (21%) of unprecedented near-term warming than for SSP1-1.9 or SSP1-2.6. Pursuing rapid, stringent mitigation therefore substantially reduces the risk of experiencing unprecedented warming rates over the next 20 years, giving societies and ecosystems a greater chance to adapt to and avoid the worst impacts of climate change. Indeed, for warming rates of 0.3 °C per decade, which is close to the threshold for unprecedented warming rates, it has been estimated that only 30% of all climate-change-impacted ecosystems and only 17% of impacted forests can adapt[24].

Note that very high near-term warming rates, which are substantially larger than the maximum observed historical 20-year trend, are still possible in all scenarios considered. However, a key point for policymakers to note is that strong mitigation greatly reduces the extremity of these low-probability high-impact cases, reducing the risk of ecosystems declining and adaptation plans failing. Under SSP5-8.5 and SSP3-7.0, the upper 5% of trends are 0.50–0.83 °C per decade and 0.43–0.79 °C per decade, respectively, while this extreme range is 0.32–0.50 °C per decade for SSP1-2.6 and 0.26–0.43 °C per decade for SSP1-1.9 (Fig. 1a; FaIR boxes). For warming rates over 0.4 °C per decade, evidence suggests that all ecosystems will decline, as they will not be able to adapt rapidly enough[25]. These extremes are caused by a combination of relatively high equilibrium climate sensitivity (ECS), high transient climate response (TCR), high ERF trends and high positive internal variability. Very low near-term warming rates are also possible in all scenarios considered. However, only under mitigation would it be possible (but very unlikely) to observe a cooling trend over the next 20 years. Only 2% of trends show near-term cooling in SSP1-1.9, where the minimum trend is −0.13 °C per decade. Maher et al.[5] found that cooling trends could be observed in the near term even under a worse-case emissions scenario, when using a shorter 15-year time horizon and considering trends at individual locations rather than the global average trend.

We now ask what the probability is, over the next 20 years, of the warming trend being lower if a mitigation pathway is followed rather than a no mitigation pathway. This is important since internal variability could overwhelm a forced temperature signal from diverging trajectories of GHG and aerosol concentrations, masking the near-term benefits of mitigation efforts. The probability that pursuing a mitigation pathway will result in a lower near-term temperature trend by a factor α as compared with following a no mitigation pathway ($P(\text{trend}_{\text{mit}} < \text{trend}_{\text{nomit}} - \alpha \times \text{trend}_{\text{nomit}})$) is shown in Table 1. The values of α are chosen to assess whether the trend is, first, lower by any amount ($\alpha = 0$) and, second, lower by a sizable amount (20% and 40%, $\alpha = 0.2$ and $\alpha = 0.4$). The probabilities for $\alpha = 0$ are calculated from the distributions created by randomly sampling with replacement from each FaIR trend distribution and taking their difference, where this is repeated $n = 10^5$ times (Fig. 2a,b). For $\alpha = 0.2$ and $\alpha = 0.4$, the probabilities are calculated by shifting the same distributions by the amount $\alpha \times \text{trend}_{\text{nomit}}$. Comparing the 1.5 °C and 2 °C scenarios (SSP1-1.9 and SSP1-2.6) with the average no mitigation scenario (SSP3-7.0; Fig. 2a), there is around a 90% and 80% probability, respectively (Table 1), that the near-term temperature trend would be lower when following the strong mitigation pathway. Under less ambitious mitigation consistent with the current and projected NDCs, the probability of the warming trend being lower than in the average no mitigation pathway is 74%. Even when the trend under mitigation is required to be at least 20% (40%) lower than under no mitigation, there is still an 83% (67%) probability of this outcome for SSP1-1.9 compared with SSP3-7.0.

A more stringent test, similar to that described by Marotzke[4] (hereafter M19), is to ask what is the probability that mitigation is both sufficient and necessary (P_{ns}) for a reduction in the temperature trend over 2021–2040 relative to the trend over the recent past. To calculate P_{ns}, the observed 20-year temperature trend for 2000–2019 ($\text{trend}_{\text{obs}}$) is subtracted from each distribution of FaIR near-term trends for the mitigation and no mitigation scenarios. Since the recently observed trend differs somewhat in multiple observational

Table 1 | The probability of experiencing different near-term (2021–2040) GSAT trends, as a result of following a mitigation pathway rather than a no mitigation pathway

Scenario comparison	$P(\text{trend}_{\text{mit}} < \text{trend}_{\text{nomit}} - \alpha \times \text{trend}_{\text{nomit}})$			$P_{\text{ns}} = P_{\text{mit}} - P_{\text{nomit}}$		
	$\alpha = 0$	$\alpha = 0.2$	$\alpha = 0.4$	P_{mit}	P_{nomit}	P_{ns}
Below 1.5 °C versus average no mitigation	0.91	0.83	0.67	0.88	0.25	0.63
Below 2 °C versus average no mitigation	0.80	0.65	0.43	0.69	0.25	0.43
NDCs versus average no mitigation	0.74	0.56	0.32	0.57	0.25	0.32
Below 1.5 °C versus worst-case no mitigation	0.96	0.90	0.77	0.88	0.12	0.76
Below 2 °C versus worst-case no mitigation	0.89	0.77	0.56	0.69	0.12	0.57
NDCs versus worst-case no mitigation	0.85	0.70	0.46	0.57	0.12	0.46

Columns 2 through 4 show the probability of the near-term temperature trend in a mitigation scenario ($\text{trend}_{\text{mit}}$) being lower than in a no mitigation scenario ($\text{trend}_{\text{nomit}}$) by a factor α ($P(\text{trend}_{\text{mit}} < \text{trend}_{\text{nomit}} - \alpha \times \text{trend}_{\text{nomit}})$). For $\alpha = 0$, the probabilities are calculated from the distributions in Fig. 2a,b; for $\alpha = 0.2$ and $\alpha = 0.4$, they are calculated by shifting the same distributions by the amount $\alpha \times \text{trend}_{\text{nomit}}$. Columns 5 through 7 show the probability, P_{ns}, that mitigation is both necessary and sufficient to experience a near-term temperature trend that is smaller than the trend observed, $\text{trend}_{\text{obs}}$, over the past 20 years (2000–2019). P_{ns} is given by $P_{\text{mit}} - P_{\text{nomit}}$, where $P_{\text{mit}} = P(\text{trend}_{\text{mit}} < \text{trend}_{\text{obs}})$ and $P_{\text{nomit}} = P(\text{trend}_{\text{nomit}} < \text{trend}_{\text{obs}})$. P_{mit} and P_{nomit} are calculated from the distributions in Fig. 2c. The probabilities are shown for mitigation pathways consistent with the current and projected NDCs, very strong mitigation in line with limiting warming to below 1.5 °C (SSP1-1.9) and strong mitigation in line with limiting warming to below 2 °C (SSP1-2.6), and no mitigation pathways consistent with an average no mitigation baseline scenario (SSP3-7.0) and a worst-case no mitigation scenario (SSP5-8.5).

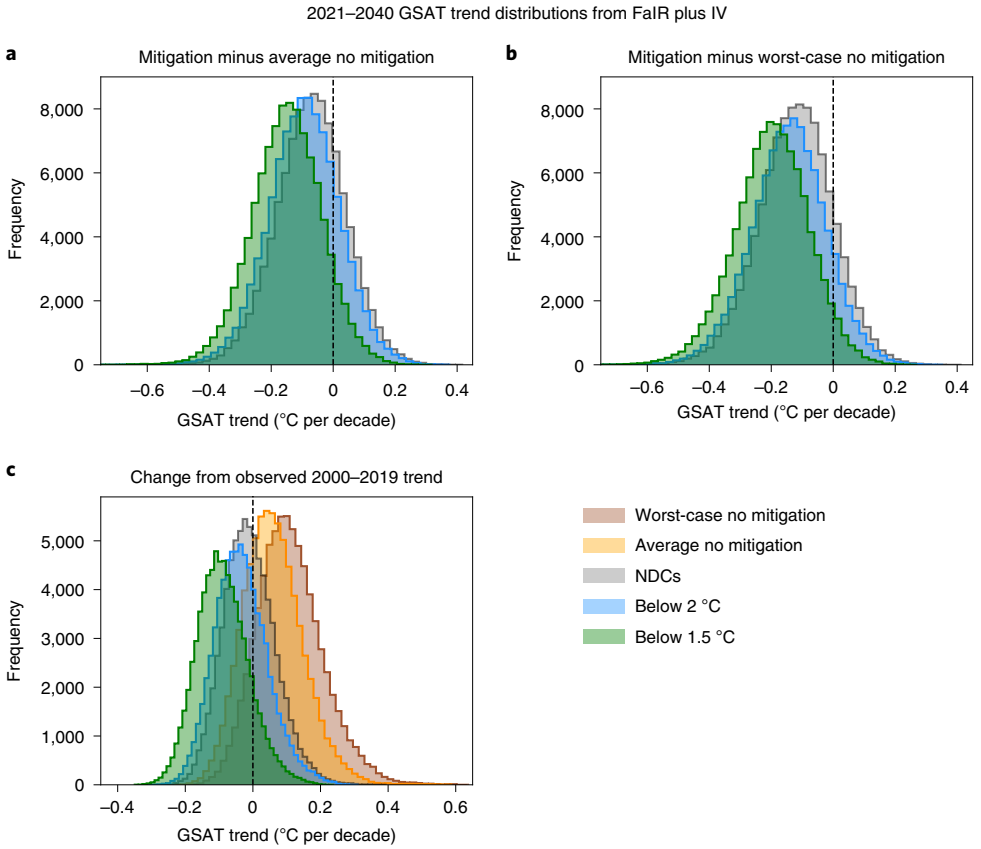

Fig. 2 | The effect of mitigation versus no mitigation on near-term (2021–2040) GSAT trend distributions from FaIR. a–c, Distributions for mitigation pathways minus an average no mitigation pathway (**a**), mitigation pathways minus a worst-case no mitigation pathway (**b**) and mitigation and no mitigation pathways minus the observed trend for the past 20 years (**c**) (2000–2019; the observational datasets used are those in Supplementary Fig. 1). The trends are calculated from FaIR projections plus an observation-based estimate of internal variability (Methods). See the main text for the details on how the distributions were calculated.

datasets (Supplementary Fig. 1), a dataset is randomly chosen for each comparison with the FaIR projections. The resulting distributions (Fig. 2c) give the probability of a trend reduction compared with the recent past under mitigation ($P_{mit} = P(\text{trend}_{mit} < \text{trend}_{obs})$) and no mitigation ($P_{nomit} = P(\text{trend}_{nomit} < \text{trend}_{obs})$) scenarios. P_{ns} is then calculated as $P_{ns} = P_{mit} - P_{nomit}$. This is similar to the approach of M19 (ref. [4]), except that here we use the observed trend, which is known, rather than a distribution of modelled trends for the recent past. Compared with the first test conducted (Table 1 and Fig. 2a,b), this more stringent test gives a lower probability of mitigation causing a reduction in the near-term temperature trend compared with no mitigation, as expected. However, for the difference between the 1.5 °C mitigation scenario and the average no mitigation scenario, the probability that mitigation is both necessary and sufficient to cause a reduction in the trend as compared with recent observations is close to 66% (Table 1).

To investigate the extent to which our results depend on the period or trend length considered, we use the FaIR emulator including estimates of internal variability to calculate warming rates for temperature trends starting in 2021 and ending in different years (Fig. 3). The 66% probability range of trends for SSP3-7.0 and SSP1-1.9 become non-overlapping after around 20 years (that is, by around 2040). This is also around the time at which the SSP5-8.5 and SSP1-2.6 66% probability ranges become separated. For SSP3-7.0 and SSP1-2.6, it takes until around 2047 for the 66% probability distributions to no longer overlap. For periods shorter than 20 years (that is, ending before 2040), the distributions of plausible warming trends between the scenarios are less distinguishable. The black line in Fig. 3 shows the maximum historical observed trend for different trend lengths based on the mean of the four datasets in Supplementary Fig. 1. The 66% probability range of trends starting from 2021 in SSP1-1.9 always falls below the maximum observed trend for all periods considered. In contrast, the median trend for SSP3-7.0 lies above the maximum observed trend for periods longer than around 18 years from the present (that is, ending after 2038).

The results presented here agree with those of Ciavarella et al.[26], where it is shown that strong mitigation markedly reduces the risk of exposure to climate extremes in the near term in an earlier generation of climate models (CMIP5; ref. [27]) driven by Representative Concentration Pathway (RCP[28]) scenarios. However, their focus is on regional extremes and local warm seasons, whereas we take a global and annual mean perspective motivated by the Paris Agreement targets. Our results do differ somewhat from the many studies that find little detectable benefit of mitigation in the near term[3–6,29,30]. This may be because these studies use model-based rather than observation-based estimates of internal variability (Supplementary Fig. 2), because they compare pathways with more similar radiative forcings[4,6,29,30] (for example, M19 (ref. [4]) considers RCP2.6 versus RCP4.5, and Samset et al.[6] focus on idealized mitigation scenarios for individual forcers rather than the combination of forcing agents in the SSPs) or because they consider shorter time horizons[4–6] (for example, M19 (ref. [4]) analyses 15-year temperature trends; Fig. 3).

In contrast to our findings for near-term temperature trends, and in agreement with the IPCC's Fifth Assessment Report (AR5; ref. [2]) where a different set of models and scenarios were compared,

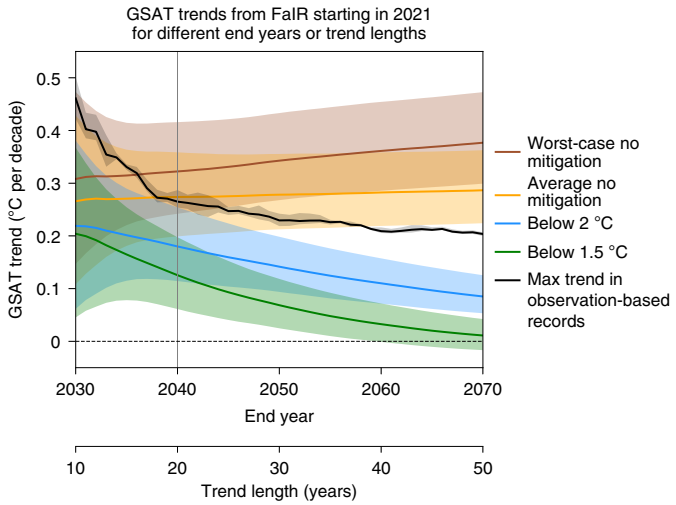

Fig. 3 | GSAT trends from FaIR starting in 2021 for different end years or trend lengths. The median trends are shown by coloured solid lines, and the 17–83% (66% probability) range in trends is shown by coloured shading. The trends are calculated from FaIR projections plus an observation-based estimate of internal variability (Methods). The data are shown for emissions pathways consistent with very strong mitigation in line with limiting warming to below 1.5 °C (SSP1-1.9, green), strong mitigation in line with limiting warming to below 2 °C (SSP1-2.6, blue), an average no mitigation baseline scenario (SSP3-7.0, orange) and a worst-case no mitigation scenario (SSP5-8.5, brown). The black shading and line show the range and mean of the maximum historical trends for different trend lengths from four different observation-based records (GISTEMPv4, CWv2 updated with HadSST3, HadCRUT4.6 and BE; see Supplementary Fig. 1). To compare with the model-simulated GSAT projections, the observation data have been converted from GBST to GSAT using a scaling factor of 1.087 for BE, CWv2 and GISTEMPv4, and 1.19 for HadCRUT4.6 (Methods). The grey vertical line highlights the year 2040, or a trend length of 20 years, which corresponds to the trend distributions for 2021–2040 shown in Fig. 1a.

our results show little difference between SSP scenarios for mean temperature anomalies (as opposed to trends) in the next 20 years (2021–2040) relative to a baseline of 1995–2014 (Fig. 1b). This holds for both the observationally constrained CMIP6 projections and the FaIR projections with added internal variability. The median 20-year mean temperature anomalies for the different SSPs all lie within 0.62–0.71 °C for the constrained CMIP6 projections (0.55–0.70 °C for FaIR), with the range about the median being determined by internal variability, differences in climate response between models and differences in ERF. Differing conclusions about the detectability of differences in temperature trends and anomalies between scenarios in Fig. 1 arise because the anomalies quantify the difference in warming between the 20-year periods centred on 2030 and 2005, while the trends quantify the difference in warming between the later years of 2040 and 2021, a period for which the different emissions pathways are more divergent (Supplementary Fig. 3).

To conclude, we have shown that rapid mitigation of global GHG emissions substantially reduces the risk of experiencing unprecedented rates of surface warming over the next two decades, even after accounting for internal variability. This is in addition to the longer-term benefits of stringent mitigation for peak warming and stabilization of climate. While it is possible that unprecedented warming rates could occur in the near term even if society pursues a path towards net-zero emissions around mid-century, the risk of such an outcome is substantially reduced by around a factor of 13 for the most ambitious mitigation scenario (SSP1-1.9) as compared with an average no mitigation scenario (SSP3-7.0).

The rate of warming over the next 20 years will determine the pace at which and extent to which societies and ecosystems will need to adapt to evolving climate hazards. On the basis of our results, under the strong mitigation scenario SSP1-2.6, the probability of crossing the threshold of 1.5 °C of anthropogenic warming in the next 20 years is around half that in SSP3-7.0 (42% compared with 78% probability; Supplementary Table 2). Furthermore, the lower near-term warming rates under SSP1-1.9 give an estimated 74% probability that the 1.5 °C threshold will never be crossed (Supplementary Table 2). The IPCC SR1.5 report[1,31] shows that warming of 1.5 °C is associated with severe and widespread impacts and risks from extreme weather events (for example, projections show extreme heat-waves becoming widespread in the tropics[32–34]; the hottest days in mid-latitudes becoming up to 3 °C warmer[35–37]; the coldest nights in the Arctic becoming up to 4.5 °C warmer[35–37]; and increases in the frequency, intensity and/or amount of heavy precipitation in several regions globally[35–37]) and from ocean warming and acidification, which are expected to impact a range of marine organisms and ecosystems (for example, 70–90% of warm-water coral reefs are projected to disappear at a warming of 1.5 °C; ref. [38]). The aggregated effect of these climate impacts and risks is projected to be the highest in regions where vulnerable populations live, particularly in South Asia[39]. The results reported here serve as further motivation for setting stringent mitigation targets to reach net-zero emissions as soon as possible on both global and individual-country levels.

Lastly, it is important to communicate what can be reasonably expected from stringent mitigation in the near term, so as to manage expectations and avoid causing doubt in the public mind about how well anthropogenic climate change is understood. In particular, while we have shown that there is a high probability that stringent mitigation would result in lower near-term warming rates compared with an average no mitigation scenario, there is a lower probability that stringent mitigation is necessary and sufficient to cause a slow-down in the warming rate in the near term compared with the recent past.

Online content

Any methods, additional references, Nature Research reporting summaries, source data, extended data, supplementary information, acknowledgements, peer review information; details of author contributions and competing interests; and statements of data and code availability are available at https://doi.org/10.1038/s41558-020-00957-9.

Received: 9 April 2020; Accepted: 26 October 2020;
Published online: 07 December 2020

References

1. IPCC: Summary for Policymakers. in *Special Report on Global Warming of 1.5 °C* (eds Masson-Delmotte, V. et al.) (WMO, 2018).
2. Kirtman, B. et al. in *Climate Change 2013: The Physical Science Basis* (eds Stocker, T. F. et al.) Ch. 11 (IPCC, Cambridge Univ. Press, 2013).
3. Tebaldi, C. & Friedlingstein, P. Delayed detection of climate mitigation benefits due to climate inertia and variability. *Proc. Natl Acad. Sci. USA* **110**, 17229–17234 (2013).
4. Marotzke, J. Quantifying the irreducible uncertainty in near-term climate projections. *WIREs Clim. Change* **10**, e563 (2019).
5. Maher, N., Lehner, F. & Marotzke, J. Quantifying the role of internal variability in the temperature we expect to observe in the coming decades. *Environ. Res. Lett.* **15**, 054014 (2020).
6. Samset, B. H., Fuglestvedt, J. S. & Lund, M. T. Delayed emergence of a global temperature response after emission mitigation. *Nat. Commun.* **11**, 3261 (2020).
7. Challinor, A. et al. Current warming will reduce yields unless maize breeding and seed systems adapt immediately. *Nat. Clim. Change* **6**, 954–958 (2016).
8. Gersonius, B. et al. Managing the flooding system's resiliency to climate change. *Proc. Inst. Civ. Eng. Eng. Sustain.* **163**, 15–22 (2010).
9. Allen, M. R. et al. in *Special Report on Global Warming of 1.5 °C* (eds Masson-Delmotte, V. et al.) Ch. 1 (IPCC, WMO, 2018).

10. Schleussner, C.-F. et al. Science and policy characteristics of the Paris Agreement temperature goal. *Nat. Clim. Change* **6**, 827–835 (2016).
11. Rogelj, J., Schleussner, C.-F. & Hare, W. Getting it right matters: temperature goal interpretations in geoscience research. *Geophys. Res. Lett.* **44**, 10662–10665 (2017).
12. Hawkins, E. & Sutton, R. The potential to narrow uncertainty in regional climate predictions. *Bull. Am. Meteorol. Soc.* **90**, 1095–1108 (2009).
13. Lehner, F. et al. Partitioning climate projection uncertainty with multiple large ensembles and CMIP5/6. *Earth Syst. Dyn.* **11**, 491–508 (2020).
14. Kosaka, Y. & Xie, S.-P. Recent global-warming hiatus tied to equatorial Pacific surface cooling. *Nature* **501**, 403–407 (2013).
15. Medhaug, I., Stolpe, M. B., Fischer, E. M. & Knutti, R. Reconciling controversies about the 'global warming hiatus'. *Nature* **545**, 41–47 (2017).
16. Meinshausen, M. et al. The shared socio-economic pathway (SSP) greenhouse gas concentrations and their extensions to 2500. *Geosci. Model Dev.* **13**, 3571–3605 (2020).
17. Tokarska, K. B. et al. Past warming trend constrains future warming in CMIP6 models. *Sci. Adv.* **6**, eaaz9549 (2020).
18. Smith, C. J. et al. FAIR v1.3: a simple emissions-based impulse response and carbon cycle model. *Geosci. Model Dev.* **11**, 2273–2297 (2018).
19. Haustein, K. et al. A limited role for unforced internal variability in twentieth-century warming. *J. Clim.* **32**, 4893–4917 (2019).
20. Rogelj, J. et al. Understanding the origin of Paris Agreement emission uncertainties. *Nat. Commun.* **8**, 15748 (2017).
21. Rogelj, J., den Elzen, M., Huppmann, D. & Luderer, G. in *Emissions Gap Report 2019* (eds Olhoff, A. & Christensen, J. M.) Ch. 3 (United Nations Environment Programme, 2019).
22. Vrontisi, Z. et al. Enhancing global climate policy ambition towards a 1.5 °C stabilization: a short-term multi-model assessment. *Environ. Res. Lett.* **13**, 044039 (2018).
23. Hausfather, Z. & Peters, G. P. Emissions—the 'business as usual' story is misleading. *Nature* **577**, 618–620 (2020).
24. Leemans, R. & Eickhout, B. Another reason for concern: regional and global impacts on ecosystems for different levels of climate change. *Glob. Environ. Change* **14**, 219–228 (2004).
25. Neilson, R. P. Transient ecotone response to climatic change: some conceptual and modelling approaches. *Ecol. Appl.* **3**, 385–395 (1993).
26. Ciavarella, A., Stott, P. & Lowe, J. Early benefits of mitigation in risk of regional climate extremes. *Nat. Clim. Change* **7**, 326–330 (2017).
27. Taylor, K. E., Stouffer, R. J. & Meehl, G. A. An overview of CMIP5 and the experiment design. *Bull. Am. Meteorol. Soc.* **93**, 485–498 (2012).
28. Meinshausen, M. et al. The RCP greenhouse gas concentrations and their extensions from 1765 to 2300. *Clim. Change* **109**, 213–241 (2011).
29. Lehner, F., Deser, C. & Sanderson, B. M. Future risk of record-breaking summer temperatures and its mitigation. *Clim. Change* **146**, 363–375 (2018).
30. Tebaldi, C. & Wehner, M. F. Benefits of mitigation for future heat extremes under RCP4.5 compared to RCP8.5. *Clim. Change* **146**, 349–361 (2018).
31. Hoegh-Guldberg, O. et al. in *Special Report on Global Warming of 1.5 °C* (eds Masson-Delmotte, V. et al.) Ch. 3 (IPCC, WMO, 2018).
32. Mahlstein, I., Knutti, R., Solomon, S. & Portmann, R. W. Early onset of significant local warming in low latitude countries. *Environ. Res. Lett.* **6**, 034009 (2011).
33. Coumou, D. & Robinson, A. Historic and future increase in the global land area affected by monthly heat extremes. *Environ. Res. Lett.* **8**, 034018 (2013).
34. Dosio, A., Mentaschi, L., Fischer, E. M. & Wyser, K. Extreme heat waves under 1.5 °C and 2 °C global warming. *Environ. Res. Lett.* **13**, 054006 (2018).
35. Seneviratne, S. I., Donat, M. G., Pitman, A. J., Knutti, R. & Wilby, R. L. Allowable CO_2 emissions based on regional and impact-related climate targets. *Nature* **529**, 477–483 (2016).
36. Wartenburger, R. et al. Changes in regional climate extremes as a function of global mean temperature: an interactive plotting framework. *Geosci. Model Dev.* **10**, 3609–3634 (2017).
37. Seneviratne, S. I. et al. Climate extremes, land–climate feedbacks and land-use forcing at 1.5 °C. *Phil. Trans. R. Soc. A* **376**, 20160450 (2018).
38. Schleussner, C.-F. et al. Differential climate impacts for policy-relevant limits to global warming: the case of 1.5 °C and 2 °C. *Earth Syst. Dyn.* **7**, 327–351 (2016).
39. Byers, E. Global exposure and vulnerability to multi-sector development and climate change hotspots. *Environ. Res. Lett.* **13**, 055012 (2018).

Methods

The GSAT projections used in this study come from two different approaches: the FaIR simple climate model emulator[18], with added observation-based estimates of internal variability[19] described below, and the latest-generation comprehensive climate models from CMIP6[40] constrained by observations[17]. In the main text, the main results regarding temperature trends are quantified using the distributions from FaIR rather than CMIP6, since FaIR is computationally inexpensive and can therefore more broadly sample parameter uncertainty than the more complex models used in CMIP6. FaIR can also be used to explore a wider range of emission scenarios, including an NDC-like scenario (not available for CMIP6) and the most ambitious mitigation scenario, SSP1-1.9 (too few CMIP6 models were available at the time of writing to generate adequate statistics). Note that the temperature trend distributions for the constrained CMIP6 models are very similar to those for FaIR, so both approaches are in good agreement. All trends were calculated using least-squares linear regression.

FaIR model. FaIR was used in the IPCC SR1.5 report[41] and uses values for ECS, TCR and a time series of ERF to make projections of GSAT. Here, distributions of near-term temperature projections for FaIR were calculated using 500 simulations for each SSP and the NDC-like scenario, using distributions of ECS, TCR and ERF that reflect our latest understanding since SR1.5.

ECS can be defined as $-F_{2x}/\lambda$, where F_{2x} is the ERF from a doubling of CO_2 and λ is the global climate feedback parameter. To construct a distribution of ECS, we use this relationship, sampling λ from a normal distribution with a mean of $-1.34\,W\,m^{-2}\,K^{-1}$ and a standard deviation of $0.28\,W\,m^{-2}\,K^{-1}$, and with F_{2x} equal to $4.01\,W\,m^{-2}$. This reproduces a distribution of ECS that is right-skewed (a long tail, which does not exclude very high ECS values) and a 5–95% range of 2–5 °C with a best estimate near 3 °C (cf. ref. [42]). The higher value of F_{2x} compared with AR5 results from an updated spectroscopic relationship for stratospherically adjusted CO_2 radiative forcing of $3.81\,W\,m^{-2}$ for a doubling of CO_2 (ref. [43]) plus tropospheric radiative adjustments that sum to $0.20\,W\,m^{-2}$ (ref. [44]), calculated using radiative kernels in ten climate models, and subtracting the land-surface warming component. The TCR is sampled to maintain a strong correlation with ECS[45], with a marginal distribution of TCR of 1.7 °C (1.2–2.4 °C, 5–95% range) that is broadly consistent with observational constraints[17]. Our sampling method allows the possibility of high ECS for modest TCR[46].

Emissions of GHGs and short-lived climate forcers are taken from the Reduced Complexity Model Intercomparison Project dataset[47], which assimilates anthropogenic and natural short-lived climate forcers[48,49] and inversions of GHG concentrations observed historically as well as those projected in SSP scenarios[16,50]. The emissions used for the NDC-like pathway are representative of the scenarios described in the United Nations Environment Programme Emissions Gap Report 2019 (ref. [21]) and of the pathways for the NDC-like projections in ref. [22]. The emissions pathways used for each SSP scenario considered and the NDC-like scenario are shown in Supplementary Fig. 3. The most ambitious (strong) mitigation scenario, SSP1-1.9 (SSP1-2.6), is associated with a mitigation rate of $-0.3\,GtC\,yr^{-1}$ ($-0.2\,GtC\,yr^{-1}$) in global net CO_2 emissions from 2021 to reach net-zero emissions in 2056 (2076). This is consistent with keeping anthropogenic warming below 1.5 °C (2 °C) with a probability of 74% (92%) (Supplementary Fig. 4 (refs. [51–53])). These pathways are therefore equivalent to the 'Below-1.5 °C' and 'Lower-2 °C' pathways considered in the IPCC SR1.5 report (that is, pathways with no or limited overshoot; see Table 2.1 in ref. [54]).

Emissions of CO_2 are converted to concentrations through a simple carbon cycle representation that is dependent on temperature and carbon uptake[55]. The carbon cycle parameters that govern the atmospheric lifetime of CO_2 (pre-industrial airborne fraction, and sensitivity of airborne fraction to increasing GSAT and total atmospheric carbon burden) are sampled from Gaussian distributions[16] that reproduce the observed CO_2 concentration of 407 ppm in 2018 in the ensemble median. Concentrations of non-CO_2 gases are calculated from a simple one-box model on the basis of atmospheric lifetimes from ref. [56]. GHG ERFs are calculated from concentrations from ref. [43] for CO_2, CH_4 and N_2O, and ref. [57] for other species. To account for tropospheric rapid adjustments, CO_2 forcing is increased by 5% and CH_4 forcing is reduced by 14% (ref. [18]), the latter case based on the behaviour of tropospheric water vapour in climate models that include short-wave forcing of methane. Simple relationships that convert aerosol and ozone precursors to forcings are also employed[58–60], as described in ref. [18]. Noting that the default CMIP6 aerosol forcing may have resulted in too little warming over the later twentieth century in some models[47,61] with a strong warming rebound in more recent years, we repeat the analysis but substitute in the aerosol ERF time series from AR5 (ref. [62]). However, this makes little difference to future near-term warming rates (Supplementary Fig. 5). Volcanic forcing is determined from the CMIP6 stratospheric sulphate optical depth (τ) time series converted to ERF at -18τ with an additive offset applied such that the mean volcanic ERF over the historical period is zero[18]. Solar forcing is taken from the CMIP6 extra-terrestrial solar flux dataset[63] using a reference time frame of 1850–1873 as recommended for CMIP6 pre-industrial control simulations. To convert solar flux anomaly to annual ERF, it is multiplied by ¼ (geometric factor) × 0.7 (planetary co-albedo).

Twelve categories of anthropogenic and natural radiative forcings are simulated using input emissions, with the best estimate and uncertainties in the pre-industrial to present-day ERF taken from AR5 (ref. [56]), with the exception being for aerosols, for which the review of ref. [64] is used for the 5–95% distribution of aerosol forcing of −2.0 to $-0.4\,W\,m^{-2}$ on the basis of a comprehensive assessment (this range of present-day aerosol ERF is also applied to the AR5 time series in Supplementary Fig. 5). The uncertainties are applied as a fraction of the present-day forcing (see Table 3 in ref. [18]). Historical (1995–2014) and projected near-term (2021–2040) trends in the median total ERF and its 12 components are shown in Supplementary Table 1.

FaIR does not include internal climate variability; therefore, the simulations described above only give the distribution of externally forced temperature trends (Supplementary Fig. 6). However, near-term warming trends will be substantially affected by internal variability (for example, see ref. [4]). To account for this, we add an observation-based estimate of internal variability to the forced temperature trends from FaIR. To estimate internal variability from the observed record, we use the approach of a recent study[19]. In this approach, a two-box impulse response model is used to calculate forced temperature changes since 1850, and this estimate is subtracted from the observational record to estimate temperature changes due to internal variability alone (Supplementary Fig. 7a,b). The resulting histogram of rolling trends for 20-year segments of the temperature residuals (Supplementary Fig. 7c,d) is then added to each of the 500 simulated temperature trends in FaIR (Supplementary Fig. 6), and a box plot is calculated (Fig. 1a). Here we use HadOST as the observational dataset because its sea surface temperatures (SSTs) are less biased than those of other datasets (for example, Berkeley Earth Land–Ocean and Cowtan–Way version 2 updated with HadSST3)[19]. However, the dataset used has little effect on the distributions of 20-year temperature trends due to internal variability (Supplementary Fig. 8a).

An alternative for estimating the range of temperature trends due to internal variability is to use the CMIP6 pre-industrial control simulations. Histograms of rolling temperature trends for 20-year segments of the control simulation for each of the 48 currently available CMIP6 models are shown in Supplementary Fig. 2 (see Supplementary Table 3 for a list of the models used). Before calculating these trends, any drift in each simulation was removed by subtracting the linear trend across the whole simulation. Clearly, there are noticeable differences in the magnitude of low-frequency temperature variability between models, where MIROC-ES2L is an example of a low-variability model and BCC-CSM2-MR a high-variability model. Adding the histogram for MIROC-ES2L to each of the 500 FaIR temperature trends gives similar distributions to using an observation-based estimate of variability (compare Supplementary Fig. 8a with Supplementary Fig. 8b(i)). The range of resulting trends is larger when using the high-variability model BCC-CSM2-MR (Supplementary Fig. 8b(ii)), but even with this high estimate of variability, strong mitigation still substantially reduces the risk of unprecedented warming. Under SSP1-1.9 (SSP1-2.6), 13% (26%) of trends are above the maximum observed historical trend, while for SSP3-7.0 (SSP5-8.5) this increases to 55% (69%).

Observation-based estimates of internal variability are also added to the distributions of temperature anomalies for FaIR in Fig. 1b. To do this, we first calculate the rolling mean for 20-year segments of the temperature residuals in Supplementary Fig. 7b. We then calculate rolling differences in these 20-year means, where (to preserve autocorrelation) the temporal separation between each pair of 20-year means is consistent with the separation between 2021–2040 and 1995–2014. The resulting histogram of differences in 20-year means of residuals is then added to the forced temperature anomalies from FaIR.

Note that the residuals in Supplementary Fig. 7b do not include natural variability due to volcanic and solar forcing, since ref. [19] includes volcanic and solar forcing in the impulse response model simulations of historical temperatures. Estimated future solar variability is included in the ERF time series used to make the FaIR GSAT projections, but forcing from possible future volcanic eruptions is not. It is therefore acknowledged that if, in the near term, solar variability is different from estimated or a large volcanic eruption occurs, near-term temperature trends will be different from those reported here.

CMIP6 models. We now describe the estimates of near-term warming trends derived from the CMIP6 models. It has been reported that some CMIP6 models simulate higher ECS values than previous versions in CMIP5, with some models simulating an ECS of up to around 5.7 °C (for example, ref. [65]). The projected raw warming rates in those models may be higher than in the past[65] and inconsistent with recent observed warming rates[17]. Additional information can be used to constrain a multimodel ensemble using so-called emergent constraints. Several studies have recently applied constraints to the CMIP6 multimodel ensemble global temperature projections using observed warming rates over the past few decades as compared with the models' historical simulations[17,61,66,67]. Here, we use the approach of ref. [17], which applies an emergent constraint on the CMIP6 model spread on the basis of the relationship between the surface warming rate over 1981–2017 and projected future warming levels ($R = 0.92$ and $R = 0.86$ for mid- and end-of-century, respectively, for SSP5-8.5). This justifies using the present-day observational trend estimates to constrain future projections. The observationally constrained CMIP6 median warming is over 10% lower by 2050 compared with the raw CMIP6 median, and over 17% lower by 2100 (ref. [17]). Constrained CMIP6 projections were not provided for SSP1-1.9 because at the time of writing, not

enough models were available to apply the emergent constraint on the basis of past warming rates.

A list of the CMIP6 models used to derive the constrained temperature trends can be found in Supplementary Table 3 (see Supplementary Table 1 in ref. [17] for a more detailed list of the models used in each SSP scenario).

Observation-based surface temperature datasets. To calculate observation-based temperature trends over the historical period, we use four datasets: HadCRUT4.6.0.0 (HadCRUT4.6; ref. [68]), Berkeley Earth Land–Ocean (BE[69]), Cowtan–Way version 2 updated with HadSST3 (CWv2; refs. [70–73]) and GISTEMP version 4 (GISTEMPv4; refs. [74,75]).

The observation-based datasets report global mean historical surface temperature anomalies, calculated using a blend of land near-surface air temperatures and SSTs (referred to here as GBST[17]). Over land, HadCRUT4.6 and CWv2 use CRUTEM4 (ref. [76]), BE uses the Berkeley Earth land-surface temperature field and GISTEMPv4 uses NOAA GHCN v.4 (ref. [77]). Over ocean, HadSST is used for HadCRUT4.6, CWv2 and BE, and GISTEMPv4 uses ERSSTv5 (ref. [78]). BE, CWv2 and GISTEMPv4 are interpolated to near-full coverage, while HadCRUT4.6 is left uninterpolated and therefore has incomplete coverage. By using several datasets, we aim to ensure that the results are not biased towards any one combination of land and ocean data.

We report the CMIP6 and FaIR model results in terms of GSAT, since this is the most relevant for future climate projections and impact assessments[79]. Since the observation-based GBST metric has been warming slower on average than GSAT[80], we apply a scaling factor to GBST that accounts for the blending bias and converts it to a GSAT equivalent, therefore allowing a like-for-like comparison between the observations and models. We use GSAT = 1.087 × GBST for BE, CWv2 and GISTEMPv4, and GSAT = 1.19 × GBST for HadCRUT4.6. These scaling factors are based on estimates derived from the CMIP5 models for fully blended GBST (applicable to BE, CWv2 and GISTEMPv4) and blended-masked GBST (applicable to HadCRUT4.6); see Table 1 in ref. [81] and Supplementary Fig. 1 in ref. [82]. Note that the results reported in this study are relatively insensitive to the exact scaling factor applied.

To calculate the observation-based estimates of internal variability in 20-year temperature trends (Supplementary Fig. 7), we use the same datasets as in ref. [19]: CWv2 (updated with HadSST4 (ref. [83]) here), BE and HadOST[19]. HadOST combines CWv2 over land with HadISST2 (ref. [84]) and OSTIA[85] data over ocean, and is interpolated to near-full coverage. To convert HadOST to a GSAT equivalent, we use the scaling factor for fully blended GBST (1.087). To account for a warm bias in SSTs around 1942–1945 due to changing SST sampling methods, correction factors have been applied over these years to the observation-based datasets in Supplementary Fig. 7 as in ref. [19].

Data availability

The data that support the findings of this study are available at https://github.com/Priestley-Centre/Near_term_warming with the identifier https://doi.org/10.5281/zenodo.4252506 (ref. [86]). This repository includes the FaIR simulation data, the constrained CMIP6 projections, the observation-based data and the observation-based estimates of internal variability (in fully processed form only). The SSP emissions datasets used in the FaIR simulations were downloaded from https://www.rcmip.org/, and the NDCs emissions dataset was provided by J. Rogelj. The constrained CMIP6 projections are based on ref. [17] and used surface air temperature data downloaded from ESGF (4 December 2019). The raw data used to calculate the observation-based estimates of internal variability are based on ref. [19] and were provided by K. Haustein. The surface air temperature data for the CMIP6 pre-industrial control simulations were obtained from the JASMIN/CEDA archive (29 July 2020). Further details of any CMIP6 data used are given in Supplementary Table 3 (refs. [87–155]).

Code availability

The FaIR model is available at https://doi.org/10.5281/zenodo.3588880 (ref. [156]). FaIR version 1.5 is used for all simulations in this paper. The code used to set up the FaIR simulations, analyse the data and produce the figures is available at https://github.com/Priestley-Centre/Near_term_warming with the identifier https://doi.org/10.5281/zenodo.4252506 (ref. [86]). Python/Matplotlib was used for all coding and data visualization; for some figures, the vector graphics editor Inkscape (available at https://inkscape.org/) was used to combine different figure parts into one file.

References

40. Eyring, V. et al. Overview of the Coupled Model Intercomparison Project Phase 6 (CMIP6) experimental design and organization. *Geosci. Model Dev.* **9**, 1937–1958 (2016).
41. IPCC *Special Report on Global Warming of 1.5 °C* (eds Masson-Delmotte, V. et al.) (WMO, 2018).
42. Dessler, A. E. & Forster, P. M. An estimate of equilibrium climate sensitivity from interannual variability. *J. Geophys. Res. Atmos.* **123**, 8634–8645 (2018).
43. Etminan, M., Myhre, G., Highwood, E. J. & Shine, K. P. Radiative forcing of carbon dioxide, methane, and nitrous oxide: a significant revision of the methane radiative forcing. *Geophys. Res. Lett.* **43**, 12614–12623 (2016).
44. Smith, C. J. et al. Understanding rapid adjustments to diverse forcing agents. *Geophys. Res. Lett.* **45**, 12023–12031 (2018).
45. Flato, G. et al. in *Climate Change 2013: The Physical Science Basis* (eds Stocker, T. F. et al.) Ch. 9 (IPCC, Cambridge Univ. Press, 2013).
46. Pfister, P. L. & Stocker, T. F. The realized warming fraction: a multi-model sensitivity study. *Environ. Res. Lett.* **13**, 124024 (2018).
47. Nicholls, Z. R. et al. Reduced complexity model intercomparison project phase 1: protocol, results and initial observations. *Geosci. Model Dev. Discuss.* https://doi.org/10.5194/gmd-2019-375 (2020).
48. van Marle, M. J. E. et al. Historic global biomass burning emissions for CMIP6 (BB4CMIP) based on merging satellite observations with proxies and fire models (1750–2015). *Geosci. Model Dev.* **10**, 3329–3357 (2017).
49. Hoesly, R. M. et al. Historical (1750–2014) anthropogenic emissions of reactive gases and aerosols from the Community Emissions Data System (CEDS). *Geosci. Model Dev.* **11**, 369–408 (2018).
50. Meinshausen, M. et al. Historical greenhouse gas concentrations for climate modelling (CMIP6). *Geosci. Model Dev.* **10**, 2057–2116 (2017).
51. Haustein, K. et al. A real-time global warming index. *Sci. Rep.* **7**, 15417 (2017).
52. Smith, T. M., Reynolds, R. W., Peterson, T. C. & Lawrimore, J. Improvements to NOAA's historical merged land–ocean surface temperatures analysis (1880–2006). *J. Clim.* **21**, 2283–2296 (2008).
53. Vose, R. S. et al. NOAA's merged land–ocean surface temperature analysis. *Bull. Am. Meteorol. Soc.* **93**, 1677–1685 (2012).
54. Rogelj, J. et al. in *Special Report on Global Warming of 1.5 °C* (eds Masson-Delmotte, V. et al.) Ch. 2 (IPCC, WMO, 2018).
55. Millar, R. J., Nicholls, Z. R., Friedlingstein, P. & Allen, M. R. A modified impulse–response representation of the global near-surface air temperature and atmospheric concentration response to carbon dioxide emissions. *Atmos. Chem. Phys.* **17**, 7213–7228 (2017).
56. Myhre, G. et al. in *Climate Change 2013: The Physical Science Basis* (eds Stocker, T. F. et al.) Ch. 8 (IPCC, Cambridge Univ. Press, 2013).
57. Hodnebrog, Ø. et al. Global warming potentials and radiative efficiencies of halocarbons and related compounds: a comprehensive review. *Rev. Geophys.* **51**, 300–378 (2013).
58. Stevenson, D. S. et al. Tropospheric ozone changes, radiative forcing and attribution to emissions in the Atmospheric Chemistry and Climate Model Intercomparison Project (ACCMIP). *Atmos. Chem. Phys.* **13**, 3063–3085 (2013).
59. Myhre, G. et al. Radiative forcing of the direct aerosol effect from AeroCom Phase II simulations. *Atmos. Chem. Phys.* **13**, 1853–1877 (2013).
60. Ghan, S. J. et al. A simple model of global aerosol indirect effects. *J. Geophys. Res. Atmos.* **118**, 6688–6707 (2013).
61. Flynn, C. M. & Mauritsen, T. On the climate sensitivity and historical warming evolution in recent coupled model ensembles. *Atmos. Chem. Phys. Discuss.* **20**, 7829–7842 (2020).
62. Prather, M. et al. (eds) in *Climate Change 2013: The Physical Science Basis* (eds Stocker, T. F. et al.) Annex II (IPCC, Cambridge Univ. Press, 2013).
63. Matthes, K. et al. Solar forcing for CMIP6 (v3.2). *Geosci. Model Dev.* **10**, 2247–2302 (2017).
64. Bellouin, N. et al. Bounding global aerosol radiative forcing of climate change. *Rev. Geophys.* **57**, e2019RG000660 (2019).
65. Forster, P. M., Maycock, A. C., McKenna, C. M. & Smith, C. J. Latest climate models confirm need for urgent mitigation. *Nat. Clim. Change* **10**, 7–10 (2020).
66. Jiménez-de-la-Cuesta, D. & Mauritsen, T. Emergent constraints on Earth's transient and equilibrium response to doubled CO_2 from post-1970s global warming. *Nat. Geosci.* **12**, 902–905 (2019).
67. Nijsse, F. J. M. M., Cox, P. M. & Williamson, M. S. Emergent constraints on transient climate response (TCR) and equilibrium climate sensitivity (ECS) from historical warming in CMIP5 and CMIP6 models. *Earth Syst. Dyn.* **11**, 737–750 (2020).
68. Morice, C. P., Kennedy, J. J., Rayner, N. A. & Jones, P. D. Quantifying uncertainties in global and regional temperature change using an ensemble of observational estimates: the HadCRUT4 dataset. *J. Geophys. Res.* **117**, D08101 (2012).
69. Rohde, R. et al. A new estimate of the average Earth surface land temperature spanning 1753 to 2011. *Geoinform. Geostat. Overv.* **1**, 1000101 (2013).
70. Kennedy, J. J., Rayner, N. A., Smith, R. O., Saunby, M. & Parker, D. E. Reassessing biases and other uncertainties in sea-surface temperature observations since 1850. 1. Measurement and sampling errors. *J. Geophys. Res.* **116**, D14103 (2011).
71. Kennedy, J. J., Rayner, N. A., Smith, R. O., Saunby, M. & Parker, D. E. Reassessing biases and other uncertainties in sea-surface temperature observations since 1850. 2. Biases and homogenisation. *J. Geophys. Res.* **116**, D14104 (2011).

72. Cowtan, K. & Way, R. G. Coverage bias in the HadCRUT4 temperature series and its impact on recent temperature trends. *Q. J. R. Meteorol. Soc.* **140**, 1935–1944 (2014).
73. Cowtan, K. D. & Way, R. G. *Global Temperature Reconstructions* Version 2 (University of York, 2020); https://doi.org/10.15124/20ee85c3-f53c-4ab6-8e50-270b0ddd3686
74. Lenssen, N. et al. Improvements in the GISTEMP uncertainty model. *J. Geophys. Res. Atmos.* **124**, 6307–6326 (2019).
75. GISTEMP Team *GISS Surface Temperature Analysis (GISTEMP)* Version 4 (NASA Goddard Institute for Space Studies, 2020); https://data.giss.nasa.gov/gistemp/
76. Jones, P. D. et al. Hemispheric and large-scale land surface air temperature variations: an extensive revision and an update to 2010. *J. Geophys. Res.* **117**, D05127 (2012).
77. Menne, M. J., Williams, C. N., Gleason, B. E., Rennie, J. J. & Lawrimore, J. H. The global historical climatology network monthly temperature dataset, version 4. *J. Clim.* **31**, 9835–9854 (2018).
78. Huang, B. et al. Extended reconstructed sea surface temperature, version 5 (ERSSTv5): upgrades, validations, and intercomparisons. *J. Clim.* **30**, 8179–8205 (2017).
79. Tokarska, K. B. et al. Recommended temperature metrics for carbon budget estimates, model evaluation and climate policy. *Nat. Geosci.* **12**, 964–971 (2019).
80. Cowtan, K. et al. Robust comparison of climate models with observations using blended land air and ocean sea surface temperatures. *Geophys. Res. Lett.* **42**, 6526–6534 (2015).
81. Richardson, M., Cowtan, K. & Millar, R. J. Global temperature definition affects achievement of long-term climate goals. *Environ. Res. Lett.* **13**, 054004 (2018).
82. Rogelj, J., Forster, P. M., Kriegler, E., Smith, C. J. & Séférian, R. Estimating and tracking the remaining carbon budget for stringent climate targets. *Nature* **571**, 335–342 (2019).
83. Kennedy, J. J., Rayner, N. A., Atkinson, C. P. & Killick, R. E. An ensemble data set of sea-surface temperature change from 1850: the Met Office Hadley Centre HadSST.4.0.0.0 data set. *J. Geophys. Res. Atmos.* **124**, 7719–7763 (2019).
84. Titchner, H. & Rayner, N. The Met Office Hadley Centre sea ice and sea surface temperature data set, version 2. 1. Sea ice concentrations. *J. Geophys. Res.* **119**, 2864–2889 (2014).
85. Donlon, C. J. et al. The operational sea surface temperature and sea ice analysis (OSTIA) system. *Remote Sens. Environ.* **116**, 140–158 (2012).
86. McKenna, C. M., Forster, P. M., Maycock, A. C., Smith, C. J. & Tokarska, K. B. *Priestley-Centre/Near_term_warming* Version 1.2 (Zenodo, 2020); https://doi.org/10.5281/zenodo.4252506
87. Dix, M. et al. *CSIRO-ARCCSS ACCESS-CM2 Model Output Prepared for CMIP6 CMIP piControl* Version 20200729 (Earth System Grid Federation, 2019); https://doi.org/10.22033/ESGF/CMIP6.4311
88. Ziehn, T. et al. *CSIRO ACCESS-ESM1.5 Model Output Prepared for CMIP6 CMIP piControl* Version 20200729 (Earth System Grid Federation, 2019); https://doi.org/10.22033/ESGF/CMIP6.4312
89. Semmler, T. et al. *AWI AWI-CM1.1MR Model Output Prepared for CMIP6 CMIP piControl* Version 20200729 (Earth System Grid Federation, 2018); https://doi.org/10.22033/ESGF/CMIP6.2777
90. Danek, C. et al. *AWI AWI-ESM1.1LR Model Output Prepared for CMIP6 CMIP piControl* Version 20200729 (Earth System Grid Federation, 2020); https://doi.org/10.22033/ESGF/CMIP6.9335
91. Wu, T. et al. *BCC BCC-CSM2MR Model Output Prepared for CMIP6 CMIP piControl* Version 20200729 (Earth System Grid Federation, 2018); https://doi.org/10.22033/ESGF/CMIP6.3016
92. Xin, X. et al. *BCC BCC-CSM2MR Model Output Prepared for CMIP6 ScenarioMIP* Version 20191204 (Earth System Grid Federation, 2019); https://doi.org/10.22033/ESGF/CMIP6.1732
93. Zhang, J. et al. *BCC BCC-ESM1 Model Output Prepared for CMIP6 CMIP piControl* Version 20200729 (Earth System Grid Federation, 2018); https://doi.org/10.22033/ESGF/CMIP6.3017
94. Rong, X. *CAMS CAMS_CSM1.0 Model Output Prepared for CMIP6 CMIP piControl* Version 20200729 (Earth System Grid Federation, 2019); https://doi.org/10.22033/ESGF/CMIP6.9797
95. Rong, X. *CAMS CAMS-CSM1.0 Model Output Prepared for CMIP6 ScenarioMIP* Version 20191204 (Earth System Grid Federation, 2019); https://doi.org/10.22033/ESGF/CMIP6.11004
96. Swart, N. C. et al. *CCCma CanESM5 Model Output Prepared for CMIP6 CMIP piControl* Version 20200729 (Earth System Grid Federation, 2019); https://doi.org/10.22033/ESGF/CMIP6.3673
97. Swart, N. C. et al. *CCCma CanESM5 Model Output Prepared for CMIP6 ScenarioMIP* Version 20191204 (Earth System Grid Federation, 2019); https://doi.org/10.22033/ESGF/CMIP6.1317
98. Danabasoglu, G., Lawrence, D., Lindsay, K., Lipscomb, W. & Strand, G. *NCAR CESM2 Model Output Prepared for CMIP6 CMIP piControl* Version 20200729 (Earth System Grid Federation, 2019); https://doi.org/10.22033/ESGF/CMIP6.7733
99. Danabasoglu, G. *NCAR CESM2 Model Output Prepared for CMIP6 ScenarioMIP* Version 20191204 (Earth System Grid Federation, 2019); https://doi.org/10.22033/ESGF/CMIP6.2201
100. Danabasoglu, G. *NCAR CESM2-FV2 Model Output Prepared for CMIP6 CMIP piControl* Version 20200729 (Earth System Grid Federation, 2019); https://doi.org/10.22033/ESGF/CMIP6.11301
101. Danabasoglu, G. *NCAR CESM2-WACCM Model Output Prepared for CMIP6 CMIP piControl* Version 20200729 (Earth System Grid Federation, 2019); https://doi.org/10.22033/ESGF/CMIP6.10094
102. Danabasoglu, G. *NCAR CESM2-WACCM Model Output Prepared for CMIP6 ScenarioMIP* Version 20191204 (Earth System Grid Federation, 2019); https://doi.org/10.22033/ESGF/CMIP6.10026
103. Danabasoglu, G. *NCAR CESM2-WACCM-FV2 Model Output Prepared for CMIP6 CMIP piControl* Version 20200729 (Earth System Grid Federation, 2019); https://doi.org/10.22033/ESGF/CMIP6.11302
104. Voldoire, A. *CMIP6 Simulations of the CNRM-CERFACS Based on CNRM-CM6-1 Model for CMIP Experiment piControl* Version 20200729 (Earth System Grid Federation, 2018); https://doi.org/10.22033/ESGF/CMIP6.4163
105. Voldoire, A. *CNRM-CERFACS CNRM-CM6-1 Model Output Prepared for CMIP6 ScenarioMIP* Version 20191204 (Earth System Grid Federation, 2019); https://doi.org/10.22033/ESGF/CMIP6.1384
106. Voldoire, A. *CNRM-CERFACS CNRM-CM6-1-HR Model Output Prepared for CMIP6 CMIP piControl* Version 20200729 (Earth System Grid Federation, 2019); https://doi.org/10.22033/ESGF/CMIP6.4164
107. Seferian, R. *CNRM-CERFACS CNRM-ESM2-1 Model Output Prepared for CMIP6 CMIP piControl* Version 20200729 (Earth System Grid Federation, 2018); https://doi.org/10.22033/ESGF/CMIP6.4165
108. Seferian, R. *CNRM-CERFACS CNRM-ESM2-1 Model Output Prepared for CMIP6 ScenarioMIP* Version 20191204 (Earth System Grid Federation, 2019); https://doi.org/10.22033/ESGF/CMIP6.1395
109. Bader, D. C., Leung, R., Taylor, M. & McCoy, R. B. *E3SM-Project E3SM1.0 Model Output Prepared for CMIP6 CMIP piControl* Version 20200729 (Earth System Grid Federation, 2019); https://doi.org/10.22033/ESGF/CMIP6.4499 (2018).
110. Bader, D. C., Leung, R., Taylor, M. & McCoy, R. B. *E3SM-Project E3SM1.1 Model Output Prepared for CMIP6 CMIP piControl*. Version 20200729. Earth System Grid Federation. https://doi.org/10.22033/ESGF/CMIP6.11489
111. Bader, D. C., Leung, R., Taylor, M. & McCoy, R. B. *E3SM-Project E3SM1.1ECA Model Output Prepared for CMIP6 CMIP piControl* Version 20200729 (Earth System Grid Federation, 2019); https://doi.org/10.22033/ESGF/CMIP6.11490
112. EC-Earth Consortium (EC-Earth) *EC-Earth-Consortium EC-Earth3 Model Output Prepared for CMIP6 ScenarioMIP* Version 20191204 (Earth System Grid Federation, 2019); https://doi.org/10.22033/ESGF/CMIP6.251
113. EC-Earth Consortium (EC-Earth) *EC-Earth-Consortium EC-Earth3-Veg Model Output Prepared for CMIP6 ScenarioMIP* Version 20191204 (Earth System Grid Federation, 2019); https://doi.org/10.22033/ESGF/CMIP6.727
114. Yu, Y. *CAS FGOALS-f3-L Model Output Prepared for CMIP6 CMIP piControl* Version 20200729 (Earth System Grid Federation, 2019); https://doi.org/10.22033/ESGF/CMIP6.3447
115. Yu, Y. *CAS FGOALS-f3-L Model Output Prepared for CMIP6 ScenarioMIP* Version 20191204 (Earth System Grid Federation, 2019); https://doi.org/10.22033/ESGF/CMIP6.2046
116. Li, L. *CAS FGOALS-g3 Model Output Prepared for CMIP6 CMIP piControl* Version 20200729 (Earth System Grid Federation, 2019); https://doi.org/10.22033/ESGF/CMIP6.3448
117. Song, Z. et al. *FIO-QLNM FIO-ESM2.0 Model Output Prepared for CMIP6 CMIP piControl* Version 20200729 (Earth System Grid Federation, 2019); https://doi.org/10.22033/ESGF/CMIP6.9205
118. Guo, H. et al. *NOAA-GFDL GFDL-CM4 Model Output piControl* Version 20200729 (Earth System Grid Federation, 2018); https://doi.org/10.22033/ESGF/CMIP6.8666
119. Guo, H. et al. *NOAA-GFDL GFDL-CM4 Model Output Prepared for CMIP6 ScenarioMIP* Version 20191204 (Earth System Grid Federation, 2018); https://doi.org/10.22033/ESGF/CMIP6.9242
120. Krasting, J. P. et al. *NOAA-GFDL GFDL-ESM4 Model Output Prepared for CMIP6 CMIP piControl* Version 20200729 (Earth System Grid Federation, 2018); https://doi.org/10.22033/ESGF/CMIP6.8669
121. John, J. G. et al. *NOAA-GFDL GFDL-ESM4 Model Output Prepared for CMIP6 ScenarioMIP* Version 20191204 (Earth System Grid Federation, 2018); https://doi.org/10.22033/ESGF/CMIP6.1414
122. NASA Goddard Institute for Space Studies (NASA/GISS) *NASA-GISS GISS-E2.1G Model Output Prepared for CMIP6 CMIP piControl* Version 20200729 (Earth System Grid Federation, 2018); https://doi.org/10.22033/ESGF/CMIP6.7380

123. NASA Goddard Institute for Space Studies (NASA/GISS) *NASA-GISS GISS-E2-1-G-CC Model Output Prepared for CMIP6 CMIP piControl* Version 20200729 (Earth System Grid Federation, 2019); https://doi.org/10.22033/ESGF/CMIP6.11856
124. NASA Goddard Institute for Space Studies (NASA/GISS) *NASA-GISS GISS-E2.1H Model Output Prepared for CMIP6 CMIP piControl* Version 20200729 (Earth System Grid Federation, 2018); https://doi.org/10.22033/ESGF/CMIP6.7381
125. NASA Goddard Institute for Space Studies (NASA/GISS) *NASA-GISS GISS-E2-2-G Model Output Prepared for CMIP6 CMIP piControl* Version 20200729 (Earth System Grid Federation, 2019); https://doi.org/10.22033/ESGF/CMIP6.7382
126. Ridley, J., Menary, M., Kuhlbrodt, T., Andrews, M. & Andrews, T. *MOHC HadGEM3-GC31-LL Model Output Prepared for CMIP6 CMIP piControl* Version 20200729 (Earth System Grid Federation, 2018); https://doi.org/10.22033/ESGF/CMIP6.6294
127. Ridley, J., Menary, M., Kuhlbrodt, T., Andrews, M. & Andrews, T. *MOHC HadGEM3-GC31-MM Model Output Prepared for CMIP6 CMIP piControl* Version 20200729 (Earth System Grid Federation, 2019); https://doi.org/10.22033/ESGF/CMIP6.6297
128. Raghavan, K. & Panickal, S. *CCCR-IITM IITM-ESM Model Output Prepared for CMIP6 CMIP piControl* Version 20200729 (Earth System Grid Federation, 2019); https://doi.org/10.22033/ESGF/CMIP6.3710
129. Volodin, E. et al. *INM INM-CM4-8 Model Output Prepared for CMIP6 CMIP piControl* Version 20200729 (Earth System Grid Federation, 2019); https://doi.org/10.22033/ESGF/CMIP6.5080
130. Volodin, E. et al. *INM INM-CM4-8 Model Output Prepared for CMIP6 ScenarioMIP* Version 20191204 (Earth System Grid Federation, 2019); https://doi.org/10.22033/ESGF/CMIP6.12321
131. Volodin, E. et al. *INM INM-CM5-0 Model Output Prepared for CMIP6 CMIP piControl* Version 20200729 (Earth System Grid Federation, 2019); https://doi.org/10.22033/ESGF/CMIP6.5081
132. Volodin, E. et al. *INM INM-CM5-0 Model Output Prepared for CMIP6 ScenarioMIP* Version 20191204 (Earth System Grid Federation, 2019); https://doi.org/10.22033/ESGF/CMIP6.12322
133. Boucher, O., Denvil, S., Caubel, A. & Foujols, M. A. *IPSL IPSL-CM6A-LR Model Output Prepared for CMIP6 CMIP piControl* Version 20200729 (Earth System Grid Federation, 2018); https://doi.org/10.22033/ESGF/CMIP6.5251
134. Boucher, O., Denvil, S., Caubel, A. & Foujols, M. A. *IPSL IPSL-CM6A-LR Model Output Prepared for CMIP6 ScenarioMIP* Version 20191204 (Earth System Grid Federation, 2019); https://doi.org/10.22033/ESGF/CMIP6.1532
135. Stouffer, R. *UA MCM-UA-1-0 Model Output Prepared for CMIP6 CMIP piControl* (Earth System Grid Federation, 2019); https://doi.org/10.22033/ESGF/CMIP6.8890
136. Hajima, T. et al. *MIROC MIROC-ES2L Model Output Prepared for CMIP6 CMIP piControl* Version 20200729 (Earth System Grid Federation, 2019); https://doi.org/10.22033/ESGF/CMIP6.5710
137. Tachiiri, K. et al. *MIROC MIROC-ES2L Model Output Prepared for CMIP6 ScenarioMIP* Version 20191204 (Earth System Grid Federation, 2019); https://doi.org/10.22033/ESGF/CMIP6.936
138. Tatebe, H. & Watanabe, M. *MIROC MIROC6 Model Output Prepared for CMIP6 CMIP piControl* Version 20200729 (Earth System Grid Federation, 2018); https://doi.org/10.22033/ESGF/CMIP6.5711
139. Shiogama, H., Abe, M. & Tatebe, H. *MIROC MIROC6 Model Output Prepared for CMIP6 ScenarioMIP* Version 20191204 (Earth System Grid Federation, 2019); https://doi.org/10.22033/ESGF/CMIP6.898
140. Neubauer, D. et al. *HAMMOZ-Consortium MPI-ESM1.2-HAM Model Output Prepared for CMIP6 CMIP piControl* Version 20200729 (Earth System Grid Federation, 2019); https://doi.org/10.22033/ESGF/CMIP6.5037
141. Jungclaus, J. et al. *MPI-M MPI-ESM1.2-HR Model Output Prepared for CMIP6 CMIP piControl* Version 20200729 (Earth System Grid Federation, 2019); https://doi.org/10.22033/ESGF/CMIP6.6674
142. Schupfner, M. et al. *DKRZ MPI-ESM1.2-HR Model Output Prepared for CMIP6 ScenarioMIP* Version 20191204 (Earth System Grid Federation, 2019); https://doi.org/10.22033/ESGF/CMIP6.2450
143. Wieners, K.-H. et al. *MPI-M MPI-ESM1.2-LR Model Output Prepared for CMIP6 CMIP piControl* Version 20200729 (Earth System Grid Federation, 2019); https://doi.org/10.22033/ESGF/CMIP6.6675
144. Yukimoto, S. et al. *MRI MRI-ESM2.0 Model Output Prepared for CMIP6 CMIP piControl* Version 20200729 (Earth System Grid Federation, 2019); https://doi.org/10.22033/ESGF/CMIP6.6900
145. Yukimoto, S. et al. *MRI MRI-ESM2.0 Model Output Prepared for CMIP6 ScenarioMIP* Version 20191204 (Earth System Grid Federation, 2019); https://doi.org/10.22033/ESGF/CMIP6.638.
146. Cao, J. & Wang, B. *NUIST NESMv3 Model Output Prepared for CMIP6 CMIP piControl* Version 20200729 (Earth System Grid Federation, 2019); https://doi.org/10.22033/ESGF/CMIP6.8776
147. Cao, J. *NUIST NESMv3 Model Output Prepared for CMIP6 ScenarioMIP* Version 20191204 (Earth System Grid Federation, 2019); https://doi.org/10.22033/ESGF/CMIP6.2027
148. Bethke, I. et al. *NCC NorCPM1 Model Output Prepared for CMIP6 CMIP piControl* Version 20200729 (Earth System Grid Federation, 2019); https://doi.org/10.22033/ESGF/CMIP6.10896
149. Guo, C. et al. *NCC NorESM1-F Model Output Prepared for CMIP6 CMIP piControl* Version 20200729 (Earth System Grid Federation, 2019); https://doi.org/10.22033/ESGF/CMIP6.11595
150. Seland, Ø. et al. *NCC NorESM2-LM Model Output Prepared for CMIP6 CMIP piControl* Version 20200729 (Earth System Grid Federation, 2019); https://doi.org/10.22033/ESGF/CMIP6.8217
151. Bentsen, M. et al. *NCC NorESM2-MM Model Output Prepared for CMIP6 CMIP piControl* Version 20200729 (Earth System Grid Federation, 2019); https://doi.org/10.22033/ESGF/CMIP6.8221
152. Park, S. & Shin, J. *SNU SAM0-UNICON Model Output Prepared for CMIP6 CMIP piControl* Version 20200729 (Earth System Grid Federation, 2019); https://doi.org/10.22033/ESGF/CMIP6.7791
153. Lee, W.-L. & Liang, H.-C. *AS-RCEC TaiESM1.0 Model Output Prepared for CMIP6 CMIP piControl* (Earth System Grid Federation, 2020); https://doi.org/10.22033/ESGF/CMIP6.9798
154. Tang, Y. et al. *MOHC UKESM1.0-LL Model Output Prepared for CMIP6 CMIP piControl* (Earth System Grid Federation, 2019); https://doi.org/10.22033/ESGF/CMIP6.6298
155. Good, P. et al. *MOHC UKESM1.0-LL Model Output Prepared for CMIP6 ScenarioMIP* Version 20191204 (Earth System Grid Federation, 2019); https://doi.org/10.22033/ESGF/CMIP6.1567
156. chrisroadmap, Gieseke, R. & Nicholls, Z. *OMS-NetZero/FAIR: RCMIP Phase 1* Version 1.5 (Zenodo, 2019); https://doi.org/10.5281/zenodo.3588880

Acknowledgements

We thank J. Rogelj for providing the NDC scenario data and K. Haustein for providing the data used to calculate the observation-based estimates of internal variability. C.M.M., A.C.M., P.M.F., C.J.S. and K.B.T. were supported by the European Union's Horizon 2020 research and innovation programme under grant agreement no. 820829 (CONSTRAIN project). A.C.M. was supported by the Natural Environment Research Council (grant no. NE/M018199/1) and Leverhulme Trust. C.J.S. was supported by a NERC/IIASA Collaborative Research Fellowship (no. NE/T009381/1). We acknowledge the World Climate Research Programme, which, through its Working Group on Coupled Modelling, coordinated and promoted CMIP6. We thank the climate modelling groups for producing and making available their model output, the Earth System Grid Federation (ESGF) for archiving the data and providing access, and the multiple funding agencies who support CMIP6 and ESGF.

Author contributions

P.M.F. and A.C.M. designed the study. C.M.M. performed the analysis and produced the figures. C.J.S. performed the FaIR simulations. K.B.T. provided the constrained CMIP6 projections. All authors contributed to writing the manuscript.

Competing interests

The authors declare no competing interests.

Additional information

Supplementary information is available for this paper at https://doi.org/10.1038/s41558-020-00957-9.

Correspondence and requests for materials should be addressed to C.M.M.

Peer review information *Nature Climate Change* thanks Daniel Huppmann, Giacomo Marangoni and the other, anonymous, reviewer(s) for their contribution to the peer review of this work.

Reprints and permissions information is available at www.nature.com/reprints.